Wind and Structures, *Vol. 26, No. 5 (2018) 317-329*
DOI: https://doi.org/10.12989/was.2018.26.5.317

Features of the flow over a finite length square prism on a wall at various incidence angles

A. Sohankar[1a], M. Kazemi Esfeh[1b], H. Pourjafari[2c], Md. Mahbub Alam[*3] and Longjun Wang[3d]

[1]*Department of Mechanical Engineering, Isfahan University of Technology, Isfahan, Iran*
[2]*Department of Mechanical Engineering, Yazd University, Yazd, Iran*
[3]*Institute for Turbulence-Noise-Vibration Interaction and Control, Shenzhen Graduate School, Harbin Institute of Technology, Shenzhen 518055, China*

(Received September 18, 2017, Revised December 7, 2017, Accepted December 9, 2017)

Abstract. Wake characteristics of the flow over a finite square prism at different incidence angles were experimentally investigated using an open-loop wind tunnel. A finite square prism with a width D = 15 mm and a height H = 7D was vertically mounted on a horizontal flat plate. The Reynolds number was varied from 6.5×10^3 to 28.5×10^3 and the incidence angle α was changed from 0^o to 45^o. The ratio of boundary layer thickness to the prism height was about δ/H = 7%. The time-averaged velocity, turbulence intensity and the vortex shedding frequency were obtained through a single-component hotwire probe. Power spectrum of the streamwise velocity fluctuations revealed that the tip and base vortices shed at the same frequency as that of spanwise vortices. Furthermore, the results showed that the critical incidence angle corresponding to the maximum Strouhal number and minimum wake width occurs at $\alpha_{cr} = 15^o$ which is equal to that reported for an infinite prism. There is a reduction in the size of the wake region along the height of the prism when moving away from the ground plane towards the free end.

Keywords: experimental study; finite square prism; incidence angle; low-speed wind tunnel; hotwire; Strouhal number

1. Introduction

The flow around infinite or two-dimensional square prisms has been widely investigated, both numerically and experimentally, over the years (Lee 1975, Igarashi 1984, Norberg 1993, Lyn *et al*. 1995, Williamson 1996, Sohankar *et al*. 1999, 2000, Duta *et al*. 2003, Sohankar 2006, 2008, Brun *et al*. 2008, Minguez *et al*. 2011, Alam *et al*. 2011, Yen *et al*. 2011, Trias *et al*. 2015, Alam *et al*. 2016, Zheng and Alam 2017). Many engineering applications, however, involve the flow around surface-mounted finite structures, such as buildings, bridges and bridge supports and power station smokestacks. The flow around such surface-mounted finite prisms is highly three-dimensional due to the end effects resulting in tip and base vortices. Fig. 1(a) shows a schematic of the flow around a surface-mounted finite square prism of width D and height H. In this figure, X, Y and Z are the coordinate axes in the streamwise, wall-normal and cross-stream directions, respectively. Here, the prism is mounted normal to a ground plane and is partially immersed in the flat-plate boundary layer, where $u(y)$ is the flow velocity in the boundary layer, $u = U$ in the freestream flow outside the boundary layer, and δ is the boundary layer thickness. For such a body, the flow field is influenced by the flow around the free end and the flow around the prism base. The local flow field thus becomes strongly three-dimensional.

The turbulent flow around a finite square prism has received less attention than the flow around an infinite prism because of its complexity. The Karman vortex shedding from the sides, the streamwise tip vortices, tip-induced downwash flow, a pair of base vortices, upwash flow from the base, and the horseshoe vortex before the base junction are the main factors for the complex wake structure of a finite prism (Fig. 1(b)).

2. Literature review

2.1 Infinite square prism at incidence

As the flow incidence angle α is varied from 0^o to 45^o, changes in time-mean drag coefficient C_D and Strouhal number St are observed, and the prism experiences a non-zero time-mean lift coefficient C_L (McClean and Sumner 2014). The main reasons for aforementioned variations are the changes in the flow separation positions and the differences in the shear layers emanating from the two sides of the prism. The other possible reasons are the shear layer reattachment on the side surfaces, rear corner interaction with shear layers, and changes in the wake width and vortex formation length (Duta *et al*. 2003, Igarashi 1984, Norberg 1993, Sohankar 2006, 2008, Wang and Zhou 2009, Adaromola *et al*. 2006).

*Corresponding author, Professor
E-mail: alam@hit.edu.cn
[a] Associate Professor
[b] Ph.D. Student
[c] MSc
[d] Ph.D. Student

http://www.techno-press.com/journals/was&subpage=7 ISSN: 1226-6116 (Print), 1598-6225 (Online)

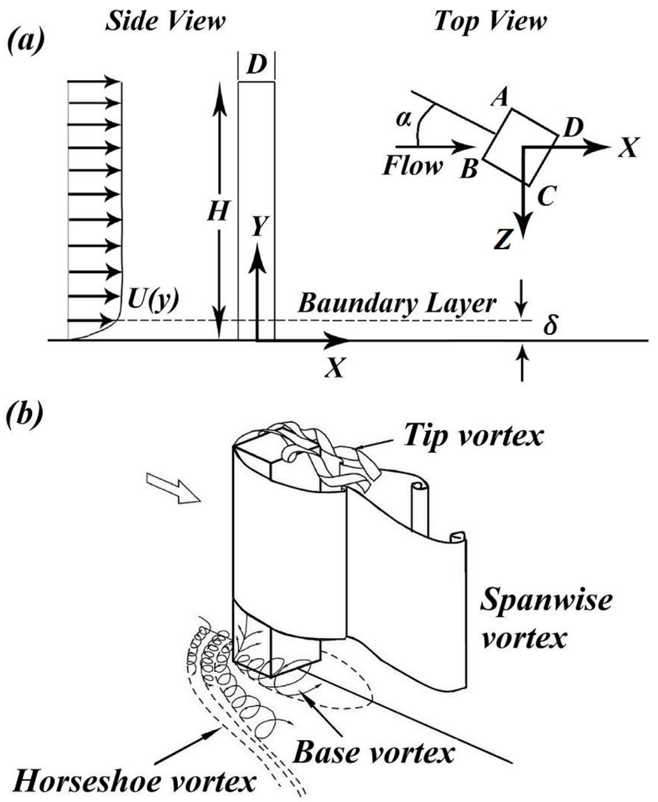

Fig. 1 Schematic of a finite square prism mounted normal to a ground plane. (a) Side and top views and (b) flow structure around a surface-mounted finite square prism (Wang and Zhou 2009)

Huang *et al*. (2010) used smoke flow visualization, surface-oil flow technique, and the resultant flow topology to identify three flow structure modes for an infinite square prism at Re = 3.4×10^4 - 9.4×10^4, and α = 0^o - 45^o. They classified the flow patterns as “subcritical flow”, where there is no reattachment of the separated shear layer onto the lower surface ($\alpha < \alpha_{cr}$), “supercritical flow”, where a separation bubble occurs on the lower surface ($\alpha > \alpha_{cr}$), and “wedge flow” (α = 45^o). In addition, they reported that the minimum wake width occurs at $\alpha = \alpha_{cr}$. Sohankar *et al*. (2015) also reported similar findings for Re = 2×10^3 - 8×10^3 via smoke flow visualization. At $\alpha = \alpha_{cr}$ the C_D and C_L attain a minimum value, and St achieves a maximum value. It should be noted that C_L is zero at α = 0^o and 45^o but negative at 0 < α < 45^o, with the minimum (most negative) occurring at $\alpha = \alpha_{cr}$. For instance, Yen and Yang (2011) obtained a minimum C_L = -0.83 at α = 13^o for Re = 3.6×10^4. The value of α_{cr} is sensitive to Re and the free stream turbulence intensity (Chen and Liu 1999, Huang *et al*. 2010, Lee 1975, Sohankar *et al*. 2015). For a low freestream turbulence intensity, α_{cr} generally lies between 11^o and 15^o. A high value of α_{cr} = 17^o has also been reported for Re = 2×10^3 - 4×10^3 (Chen and Liu 1999).

2.2 Finite square prism

The boundary layer thickness, Re, α and the prism aspect ratio AR (= H/D) are some of the parameters that influence the flow field of a finite square prism. The following section demonstrates briefly some of the main flow features of finite square prisms.

End effect: The free end of a finite cylinder is one of the main sources of the three-dimensionality of the flow. The free end alters the vortex formation region, vortex-shedding pattern and the surface pressure distribution (Yen and Yang 2012). The free end creates tip vortices, which induces a downward-directed flow known as the downwash flow (Adaromola *et al*. 2006). Around the junction of the cylinder, an adverse pressure gradient is produced. Consequently, the boundary layer is forced to separate from the ground plane, and ultimately horseshoe vortices form wrapping around the base of the cylinder. These vortices carry on moving with the stream towards the downstream (Park and Lee 2000). The size of a horseshoe vortex decays with increasing H (Okamoto and Sunabashiri 1992).

Aspect ratio effect: A finite cylinder of a small AR (less than the “critical AR”) has a wake structure different from that of a higher AR (Okamoto and Sunabashiri 1992, Adaromola *et al*. 2006). For finite cylinders greater than the critical AR, the flow pattern is characterized by the presence of the anti-symmetric Kármán vortex shedding. On the other hand, for cylinders less than the critical AR, the wake often features symmetric “arch vortex shedding”. Adaramola *et al*. (2006) and Sumner *et al*. (2004) suggested that the critical AR of a finite circular cylinder lies between AR = 3 and 5. McClean and Sumner (2014) at Re = 7.2×10^4

investigated the effects of AR (= 3 - 11) and α (= 0° - 45°) on C_D, C_L and St for a surface-mounted finite square prism. The C_D, C_L, and St are found to be very sensitive to α. This is similar to what observed for infinite square prisms. For all AR tested, the α_{cr} was 15° - 18°, higher than the typical α_{cr} range for infinite square prisms. Wang *et al*. (2004) studied the flow over a surface-mounted finite square prism of AR = 3 - 7. A broad-banded peak in the power spectrum at St = 0.09 was obtained for AR = 3, while pronounced sharp peaks at St = 0.12 and 0.13 were observed for AR = 5 and 7, respectively. For an infinite square prism, St = 0.135 was reported.

Boundary layer thickness effect: Besides AR, the δ affects the formation of the base vortices and upwash flow. For a thicker boundary layer, the base vortices are stronger and the upwash flow is more effective. The stronger upwash flow also affects the flow around the free end region, preventing the downwash flow to reach the ground plane and weakening tip vortices (Wang *et al*. 2006). Sakamoto and Arie (1983) investigated that, with increasing δ, the St decreases for all rectangular prisms.

Wang *et al*. (2006) studied the effect of δ on the flow around a finite square prism of AR = 5. They showed that δ has a significant effect on the formation and size of the base vortices. Both symmetric and anti-symmetric vortices are identified in the near wake of the prism for a given AR. The probability of anti-symmetrical vortex shedding varies with AR and δ. It considerably increases with increasing δ, particularly near the base of the prism.

Incidence angle effect: Sarode *et al*. (1981) measured C_D and C_L for surface-mounted finite square prisms of AR = 1.14 to 10 at $Re = 2.2\times10^4$. The prisms were immersed in an atmospheric boundary layer. They found that the effect of α on C_D is significant for the more slender prisms (i.e., AR = 6.36 and 10), while the effect is less significant for the smaller AR (= 1.14, 2.27, and 3.64). In addition, as AR decreases, C_L around the critical α reduces in magnitude (Sarode *et al*. 1981).

***Re* effect:** Lim *et al*. (2007) demonstrated that even at a high Re the long-standing belief in Re similarity in bluff-body flows is questionable. Owing to a reduction in the flow velocity near the base surface, the flow regime is Re dependent. Rastan *et al.* (2017) numerically examined the flow over a finite prism of AR= 7 at Re = 40-250. They identified five flow regimes, namely steady ($Re \leq 75$), transition from steady to unsteady ($75 < Re < 85$), laminar ($85 \leq Re \leq 150$), transition from laminar to turbulent ($150 < Re \leq 200$), and turbulent ($Re > 200$). While the steady flow corresponds to a dipole wake, the unsteady flow complements a quadrupole wake. The onset of vortex shedding prevails at $75 < Re < 85$ which is higher in comparison with that (Re = 51) of the infinite square prism (Sohankar *et al.* 1998). An increase in Re gives rise to a transmutation of the periodic large-scale structures at Re = 150 to the chaotic small-scale structures at Re = 250.

There are limited studies on the turbulent wake of a finite square prism. Therefore, there is a need for further studies that would provide more insight into the turbulent wake of finite structures. This study aims to investigate experimentally the flow around a wall-mounted finite square prism at $\alpha = 0^o - 45^o$ in order to gain a better understanding of the main feature of the flow structure, particularly, the effect of α on the vortex shedding. Here we provide new information on the Strouhal number data in order to extend the results in the literature (Sorode *et al*. 1981, Sakamoto 1985, McClean and Sumner 2014). To find the flow field features over a finite square prism, the turbulent wake structure including time-averaged velocity and turbulence intensity is extensively studied, using the data extracted from a hotwire anemometry. The experiments, performed in a wind tunnel, cover a relatively wide range of $Re = 6.5\times10^3$- 28.5×10^3 and of $\alpha = 0^o - 45^o$ for AR = 7.

3. Experimental set-up

Flow measurements were performed in an open return wind tunnel with a test section height, width and length of 46, 46 and 120 cm, respectively. The sidewalls of the section are made of Plexiglas thereby aiding the visualization of the experimental apparatus. The designed maximum flow speed in the wind tunnel is approximately 30 m/s. The contraction ratio between the settling chamber and test section is 5:1. A honeycomb and three turbulence reduction screens are located at the inlet-settling chamber to reduce the turbulence intensity to less than 0.3% in the test section. The non-uniformity of the flow velocity across the test-section was less than 1.5%.

A smooth steel square prism of a width D = 15 mm and an aspect ratio AR = 7 was used throughout the experiments. The square prism had sharp edges on all sides. The blockage ratio (the ratio of the frontal area of the prism to the cross-sectional area of the test section) ranges from 0.7% (for $\alpha = 0^o$) to 1.1% (for $\alpha = 45^o$) and hence the wind tunnel walls effects on the measured quantities is negligible (McClean and Sumner 2014, West and Apelt 1982).

The wind tunnel test section is equipped with a three-axis traverse system, which is controlled by a LabVIEW computer program. The traverse system is mounted above the wind tunnel such that the hotwire probe holder can enter into the wind tunnel through the ceiling as shown in Fig. 2. Three step motors are used in the traversing mechanism to control the vertical and horizontal position of the measurement probe of the hotwire system with an accuracy of ±0.1 mm.

The time-mean and fluctuating streamwise velocities were measured using a single hotwire probe. The probe was calibrated both statically and dynamically, and all data were low-pass filtered. Data were recorded via a 12-bit A/D board. In order to quantify the uncertainty of the hotwire measurement, the methodology provided by Jorgenson (2002) and Yavuzkurt (1984) was followed. The uncertainty of the results obtained with the CTA anemometer is a combination of the uncertainties of the individually acquired voltages converted into velocity. The uncertainty of each individual velocity sample was determined by non-statistical means based on detailed knowledge of the

Fig. 2 Wind tunnel test section and traverse mechanism

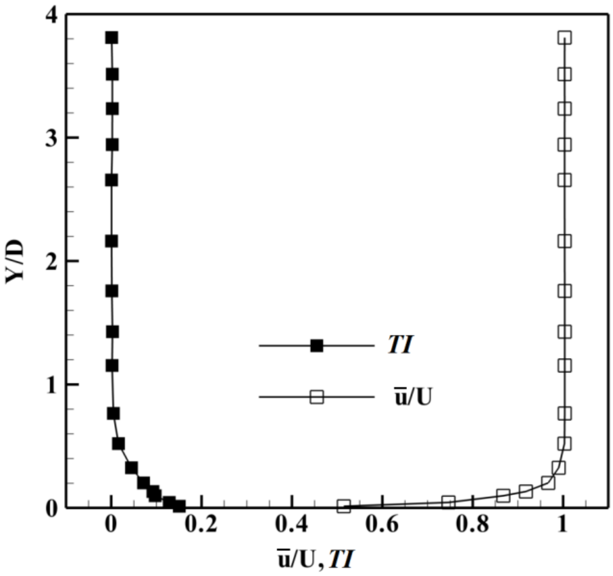

Fig. 3 Distributions of time-averaged streamwise velocity ($\overline{u}/U$) and turbulence intensity (TI) in the wind tunnel, in the absence of the prism

instrumentation, calibration and experimental conditions. The hotwire anemometer has a negligible drift, low noise, and good repeatability so that these factors do not add significantly to the uncertainty in comparison with other error sources (Jorgenson 2002). The turbulence intensity (TI) is calculated as the root-mean-square of the fluctuating streamwise velocity normalized by the freestream velocity, i.e. TI = u_{rms}/U. Bruun (1996) identified that the relative error in the measurement of turbulence intensity is less than 5% for a flow with TI = 30%. In the present study, the maximum turbulence intensity in the wake region is 27%. The measured uncertainties of the time-average velocity and turbulence intensity are less than 3.6% and 6%, respectively, in the present measurements.

Measurements of the boundary layer velocity profiles and properties were made at a freestream velocity of U = 20 m/s. The time-averaged streamwise velocity $\overline{u}/U$ and TI distributions at the location of the prism (with the prism removed) are shown in Fig. 3. The hotwire sensor was first positioned 1 mm above the surface and then traversed upward at predetermined increments. The value of TI at the first measured point, closest to the wall, is 0.15. The boundary layer thickness at U = 20 m/s is δ = 7.5 mm at the prism location (Fig. 3), corresponding to δ/D = 0.5 and δ/H = 0.07 which are negligibly small when compared with the height of the square prism. Therefore, the effect of δ on the wake structure can be ignored.

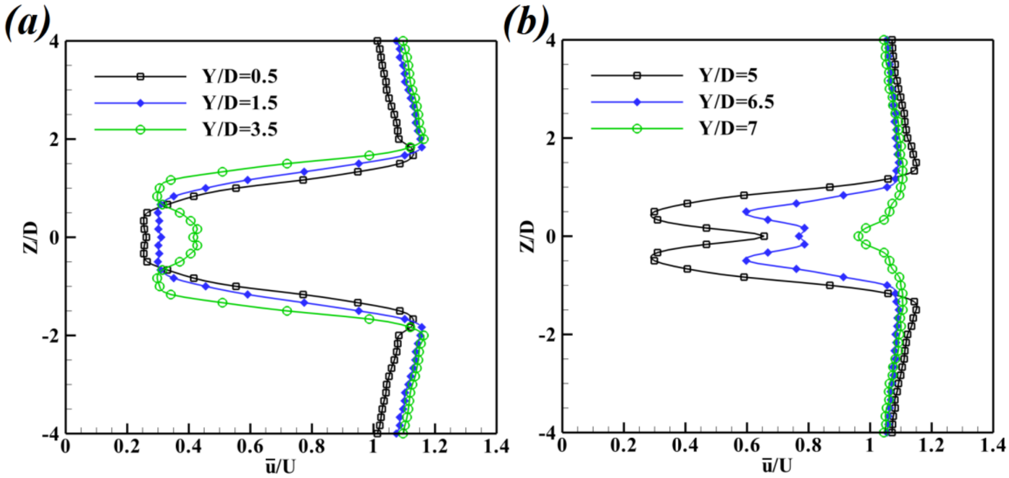

Fig. 4 Time-averaged velocity $\bar{u}/U$ distributions along the spanwise direction (Z) at Y/D = 0.5-7 (X/D = 3): (a) lower half of the prism and (b) upper half of the prism. $\alpha = 0^o$ and $Re = 2\times10^4$

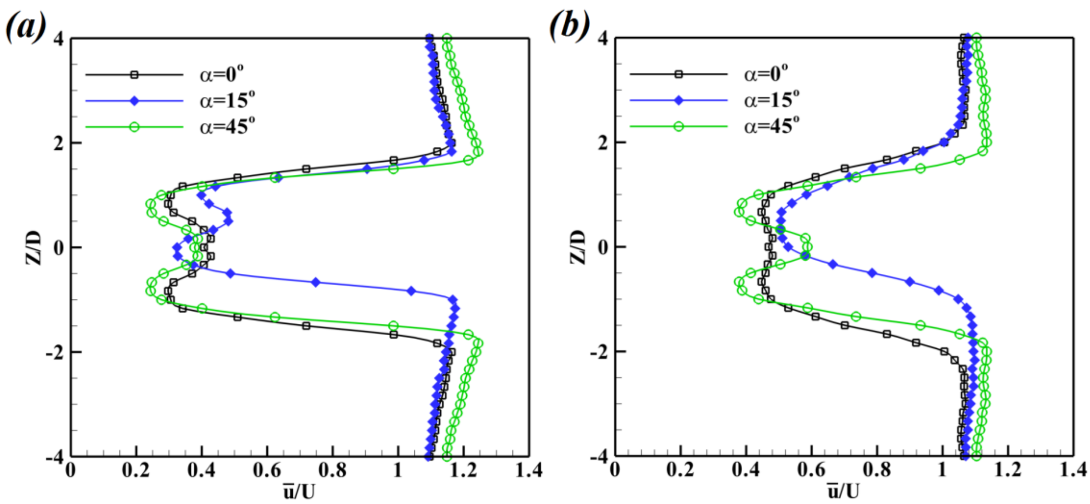

Fig. 5 Time-mean streamwise velocity $\bar{u}/U$ distributions along the spanwise direction (Z) at various α (Y/D = 3.5). (a) X/D = 3, and (b) X/D = 5. $Re = 2\times10^4$

4. Results and discussion

4.1 Mean flow field

One of the characteristics of the flow around a finite prism is that the wake structure changes significantly from the tip to the base of the prism. Fig. 4 presents $\bar{u}/U$ distribution at $\alpha = 0^o$ along the spanwise direction for various Y/D at X/D = 3, $Re = 2\times10^4$. Recall that the origin of the coordinate system is at the cylinder center on the wall (Fig. 1). The $\bar{u}/U$ distributions for Y/D = 3.5 - 6.5 display two peaks. The value of $\bar{u}/U$ is small in the region of -1.5 < Z/D < 1.5, increasing with Y/D. The appearance of two peaks in some Y/D is due to the effect of the downwash flow from the free end (Adaramola *et al*. 2006; Okamoto and Sunabashiri 1992). The downwash flow descending into the wake extends to the mid-height of the prism, and the wake flow is, therefore, divided into two similar regions. This is a cause of two peaks. It seems that near the ground plane (Y/D = 0.5 and 1.5) the $\bar{u}/U$ distribution has a single peak. This is due to the fact that the flow field close to the ground plane (Y/D < 3.5) is not influenced by the downwash flow. Fig. 4 also shows that $\bar{u}/U$ at Z/D = 0 increases from about 0.2 at Y/D = 0.5 (close to the wall) to 1.0 at Y/D = 7 (close to the ceiling).

Fig. 5 presents $\bar{u}/U$ distributions across the wake for three different incidence angles ($\alpha = 0^o, 15^o, 45^o$) at X/D = 3 and 5 at the mid-span (Y/D = 3.5) of the prism. At X/D = 3, all $\bar{u}/U$ distributions have two peaks (Fig. 5(a)). As mentioned before, these peaks are due to the downwash flow originating from the free end. It is likely that at X/D = 5 the downwash flow does not reach the mid-section (Y/D = 3.5) at $\alpha = 15^o$, the $\bar{u}/U$ having only a single peak (Fig. 5(b)).

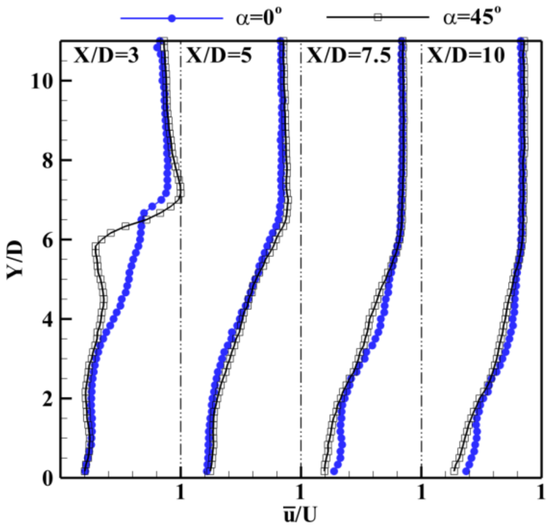

Fig. 6 Time-averaged streamwise velocity $\bar{u}/U$ distributions on the *X-Y* plane at wake center plane (*Z/D* = 0) for α = 0° and 45°. *Re* = 2×10^4

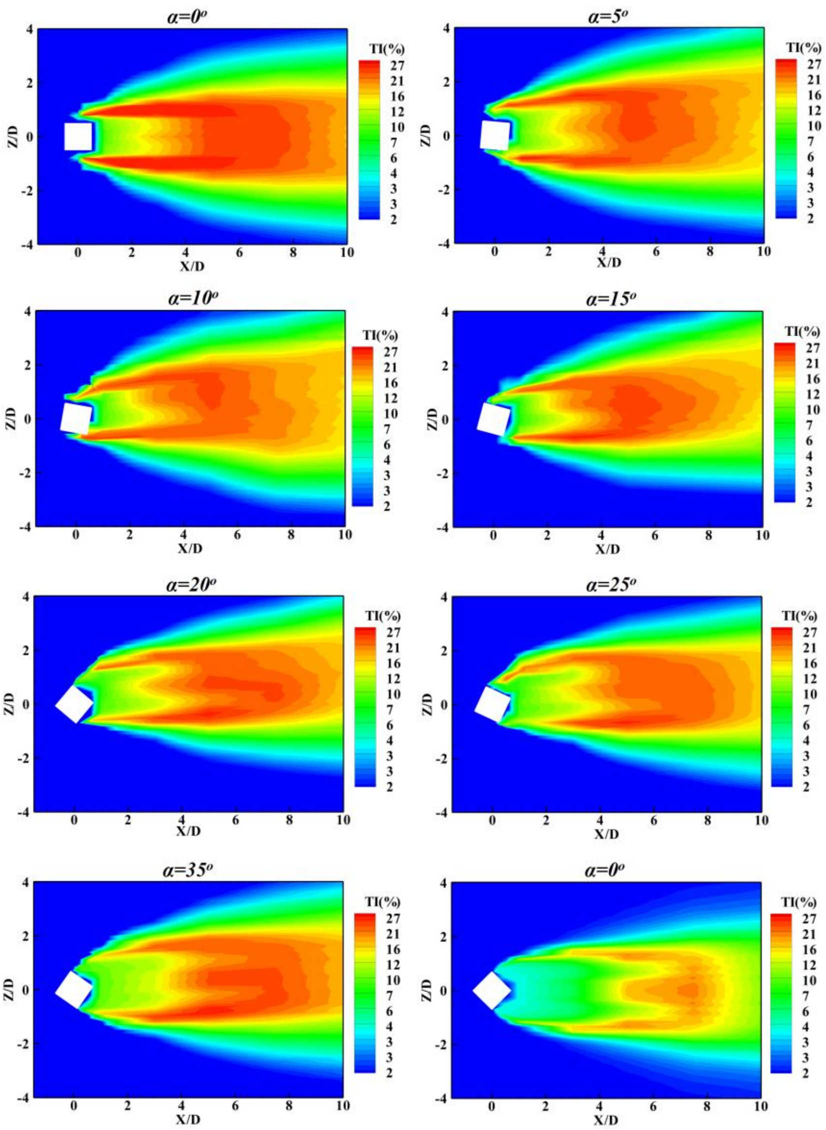

Fig. 7 Turbulence intensity (TI) contour at the mid-span plane (*Y/D* = 3.5) for various incidence angles (*Re* = 2×10^4)

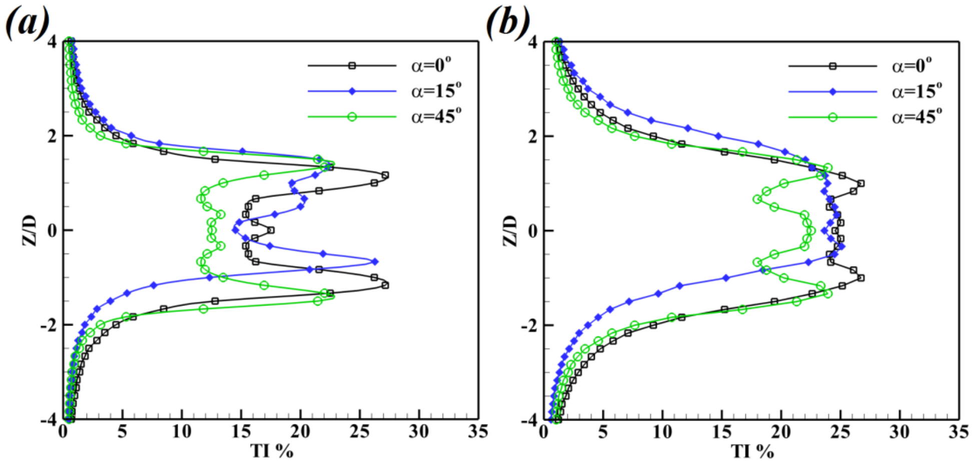

Fig. 8 Turbulence intensity distributions along the spanwise direction (Z) at various incidence angles at (a) X/D = 3, and (b) X/D = 5. Y/D = 3.5 and $Re = 2\times10^4$

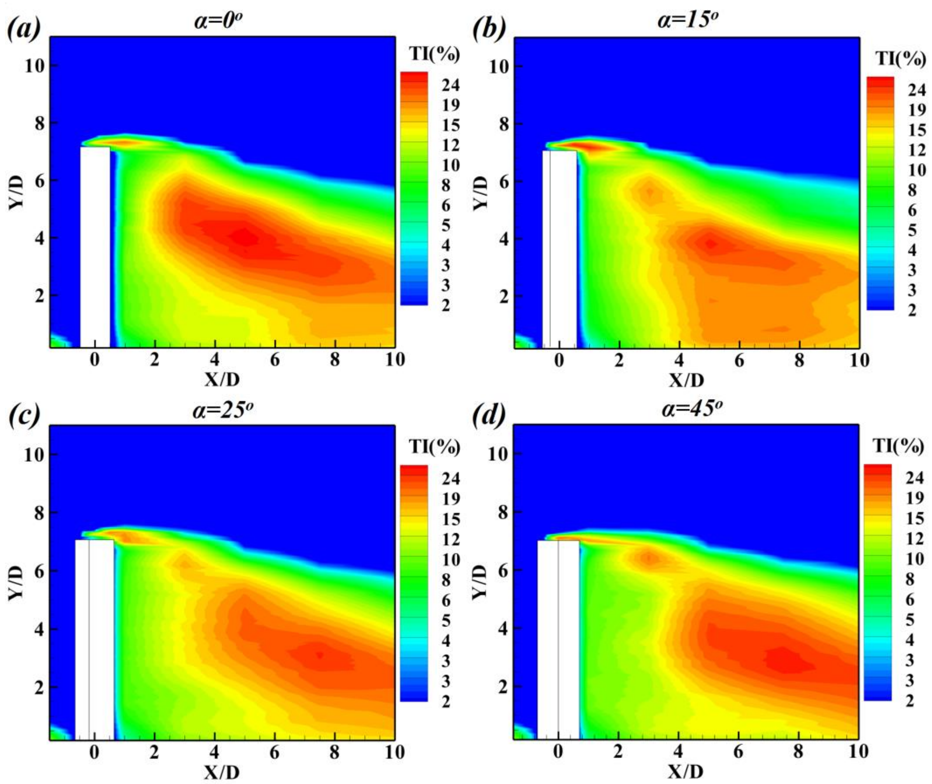

Fig. 9 Turbulence intensity contours on the X-Y plane at the wake center plane (Z/D = 0). (a) $\alpha = 0^{\circ}$, (b) $\alpha = 15^{\circ}$, (c) $\alpha = 25^{\circ}$ and (d) $\alpha = 45^{\circ}$. $Re = 2\times10^4$

Fig. 6 presents $\bar{u}/U$ distributions on the X-Y plane at Z/D = 0 for $\alpha = 0^{\circ}$ and 45°. Although $\bar{u}/U$ distributions for the two cases are roughly similar to each other at X/D = 5, 7.5 and 10, those are markedly different from each other at X/D = 3. Interestingly, the $\bar{u}/U$ distributions at X/D = 3 have relatively large variations near the free end of the cylinder (Y/D = 7), where a strong separated free shear layer forms. This shear layer engenders a downwash flow behind the cylinder. The separated shear layer and the corresponding large velocity gradient near the free end are more notable for $\alpha = 45^{\circ}$ than for $\alpha = 0^{\circ}$. Presently, the value of $\bar{u}/U$ in the wake region at X/D = 3 is still higher than zero (Figs. 4-6), implying that the saddle point (the verge of the recirculation) lies upstream of X/D = 3. Wang and Zhou (2009) at $Re = 9.3\times10^3$ observed that the reverse flow zone extends up to a maximum of X/D = 2 along the height of a finite cylinder.

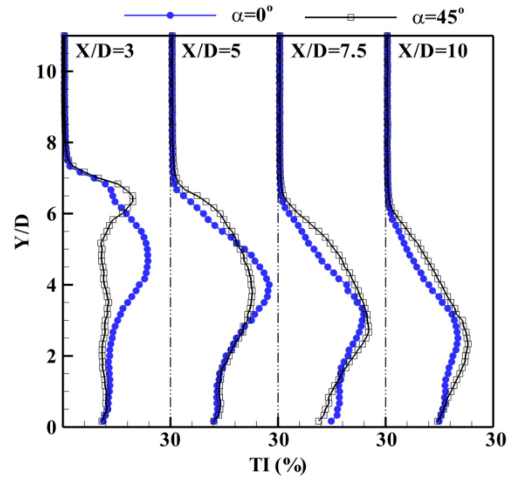

Fig. 10 Turbulence intensity distributions on the *X*-*Y* plane at wake center plane (*Z*/*D* = 0) at *X*/*D* = 3, 5, 7.5 and 10 for α = 0° and 45°. *Re* = 2×10^4

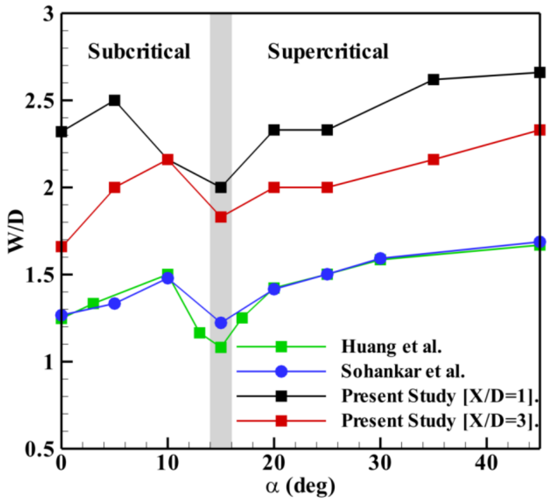

Fig. 11 Dependence of wake width (at *Y*/*D* = 3.5, *X*/*D* = 1, 3) on α (*Re* = 2×10^4). Huang *et al*.'s (2010) and Sohankar *et al*.'s (2015) results are for infinite prism, measured at *X*/*D* = 1/4 and 1.0, respectively

Turbulence intensity (TI) contours for α = 0° - 45° are presented in Fig. 7. In general, the turbulence intensity increases in the wake region with an increase in *X*/*D*, attaining a maximum at 3 < *X*/*D* < 8 before decaying. The turbulence structure experiences substantial changes with increasing α. The turbulence intensity is symmetric with respect to the symmetric plane (*Z*/*D* = 0) at α = 0°. With increasing α from α = 0° to 15°, the asymmetry in the turbulence structure grows. The asymmetry is alleviated with a further increase in α, turbulence structure eventually becoming symmetric at α = 45°. The turbulent wake of a finite square prism is dramatically different from an infinite square prism. Oudheusden *et al*. (2008) for an infinite square prism revealed that the maximum turbulence intensity is located on the lateral sides while the maximum turbulence intensity presently occurs in the shear layers separated from the leading edges (near the lateral sides) and behind the prism owing to the downwash flow.

Fig. 8 illustrates the turbulence intensity profiles for α = 0°, 15°, 45° at *Y*/*D* = 3.5 and at *X*/*D* = 3 and 5. Two peaks are observed on the shear layers at both *X*/*D* = 3 and 5 for all α at -1.5 < *Z*/*D* < 1.5. In addition, the turbulence intensity levels and its maximum decreases gradually with increasing α, with the maximum turbulence intensity at α = 0° and 45° being 27% and 24%, respectively.

Fig. 9 shows the turbulence intensity on the *X*-*Y* plane at *Z*/*D* = 0 for various α, providing a useful insight into the wake region. As can be seen from the figure, the turbulence intensity contours have two local maxima. The first one with TI = 19% - 24% is located just on the shear layer above the free end surface and the other one with TI = 24% - 27% is located behind the prism.

In order to make a detailed comparison between turbulence intensities at different α, turbulence intensity distributions on the *X*-*Y* plane at α = 0° and 45° are provided in Fig. 10. It is seen from Figs. 9 and 10 that the location of

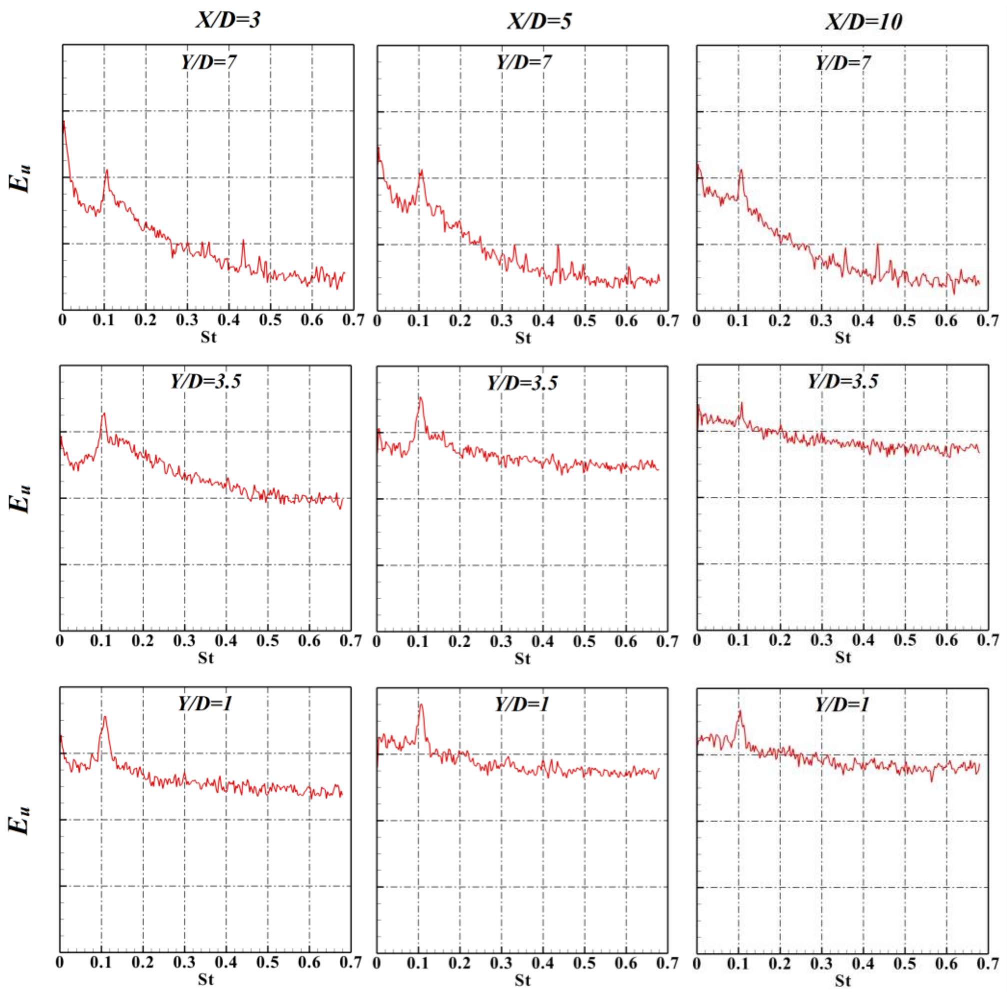

Fig. 12 Power spectra of fluctuating streamwise velocities measured at various positions along the height (Y/D = 1, 3.5, 7) for X/D = 3, 5, and 8 at Z/D = 2. $\alpha = 0^o$, and $Re = 1.1\times10^4$

the maximum turbulence intensity in the wake region moves farther downstream with increasing α. For instance, the turbulence intensity reaches a peak value of 26% ($\alpha = 0^o$) at (X/D, Y/D) = (5, 4) and 24% ($\alpha = 45^o$) at (X/D, Y/D) = (7.5, 2.75). It is observed that, at X/D = 10, the turbulence intensity distributions at $\alpha = 0^o$ and 45^o have almost a similar trend.

The wake width W was determined by Huang *et al.* (2010) and Sohankar *et al.* (2015) for an infinite square prism at various incidence angles ($Re = 6.78\times10^3$ - 7.7×10^4). Huang *et al.* (2010) and Sohankar *et al.* (2015) measured the wake width at D and $D/4$ downstream of the cylinder center, respectively. They illustrated that two local minimum wake widths occur at $\alpha = 0^o$ and 15^o, respectively. The local wake width is about 1.25D at $\alpha = 0^o$ where the cross-stream width of the square prism is minimum while it reaches to about 1.2D at the critical incidence angle $\alpha_{cr} = 15^o$ (Sohankar *et al.* 2015). The reduction in the wake width at $\alpha_{cr} = 15^o$ is attributed to the occurrence of the shear layer reattachment on the lower face (Sohankar *et al.* 2015). The shear layer passing closer to the body leads to a smaller the wake width. As the α increases from 15^o to 45^o, the wake width grows and reaches a maximum of 1.7D at $\alpha = 45^o$. When the wake width is scaled with the cylinder projection width at each incidence angle, the normalized wake width is about 1.25, 0.98 and 1.21 for $\alpha = 0^o$, $\alpha = 15^o$ and $\alpha = 45^o$, respectively (Sohankar *et al.* 2015).

In this study, the method employed by Huang *et al.* (2010) is used to estimate the wake width for a finite prism. Huang *et al.* (2010) for an infinite prism stated that the peak turbulence intensities are located in the shear layers.

Therefore, the lateral distance between the two peaks at each X/D could be used as an appropriate index for estimating the wake width. It could be noted that the features of vortex formation and wake structure for a finite cylinder are different from those for an infinite cylinder (Huang *et al.* 2010, Sohankar *et al.* 2015). Nevertheless, some similarities can be found between them; the flow pattern at the midspan of the finite prism may resemble that of an infinite cylinder due to a quasi-periodic shedding that is nominally parallel to the prism axis (Bourgeois *et al.* 2011). The scaled wake width (W/D) is shown for various incidence angles in Fig. 11 and compared with the results of Huang *et al.* (2010) and Sohankar *et al.* (2015). Despite the fact that the variation in the wake width of the finite square prism is not exactly identical to the infinite square prism,

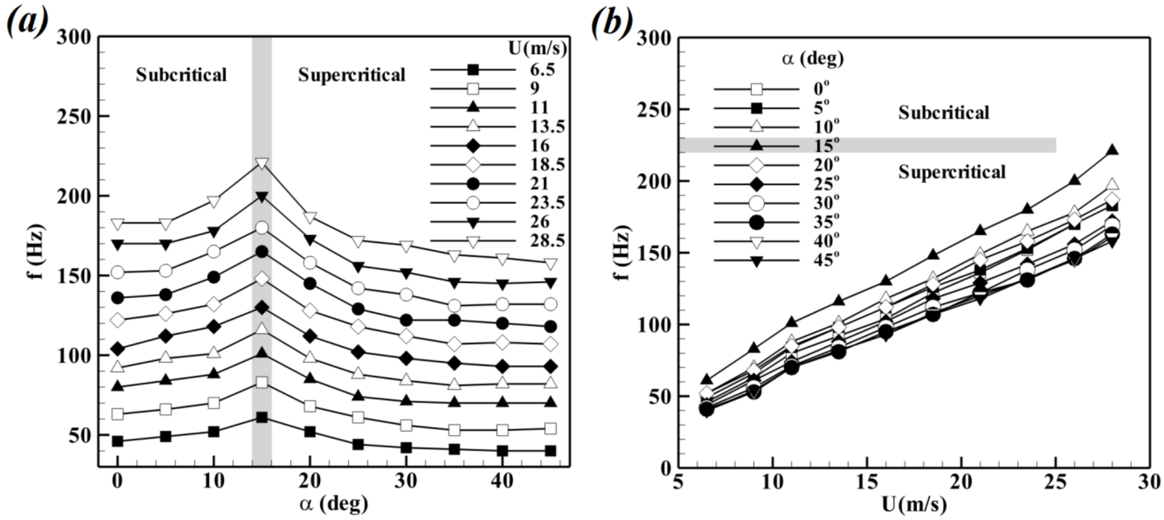

Fig. 13 Variations in shedding frequency with (a) incidence angle for various freestream velocities, and (b) inflow velocity for various incidence angles

the minimum wake width occurs at the critical incidence angle (α = 15°) and the maximum wake width appears at α = 45°. Furthermore, at all incidence angles, the wake width of the finite square prism is larger than that of the infinite one.

4.2 Strouhal number

Fig. 12 presents the variation of *St* measured using a hotwire along the height of the finite prism at three different streamwise locations for α = 0°. The hotwire probe at *Z*/*D* = 2 was varied from *Y/D* = 1 to 7 for *X/D* = 3, 5 and 10 each. The measurements were made at a freestream velocity of *U* = 11 m/s, corresponding to a *Re* = 1.1×10^4. The central frequency of the local maximum spectrum amplitude corresponds to the frequency of the vortex shedding. Notable variations are observed in the shape and strength of the peaks in the power spectra along the height of the cylinder. Fig. 12 indicates that the energy at the dominant peak declines near the free end due to the interaction between downwash flow from the free end and spanwise vortex shedding as reported by Okamato and Sunabashiri (1992).

Fig. 12 further shows that *St* = 0.107 is dominant for the nine positions considered. Wang and Zhou (2009) also obtained identical power spectra at different streamwise locations. They stated that the predominant peak occurs at the same frequency throughout the cylinder span. This implies that the tip and base vortices may shed from the cylinder at the same frequency as spanwise vortices (Wang and Zhou 2009). McClean and Sumner (2014) conducted hotwire measurements to examine how the Strouhal numbers and power spectra vary along the height of square prisms for different *AR* and α. They for *AR* = 11 and α = 0° detected *St* = 0.10 along the entire height of the prism. A similar observation was made for α = 15° where *St* = 0.12. The Strouhal peak was wider for α = 15° than for α = 0°. For *AR* = 7, Strouhal peaks were sharp for the entire height of the prism at α = 0°. When α was increased to15°, 30° and 45°, the peak was weaker and broad banded for the measured positions near the ground plane and near the free end.

The *St* = 0.107 in this work is lower than that (0.125～0.13 at *Re* = $1\times10^3\sim2\times10^4$) of an infinite prism (Okajima 1982). Zdravkovich (2003) attributed the decrease in the *St* of the finite cylinder to the free-end downwash flow. He suggested that the downwash flow elongates the vortex formation length and widens the near wake, thus prolonging the spanwise vortex shedding.

Figs. 13(a) and 13(b) shows variations in vortex shedding frequency obtained from power spectra when α is changed from 0° to 45° (with an increment of 5°) and *U* is varied from 6.5 m/s to 28.5 m/s (*Re* = 6.5×10^3 - 28.5×10^3). The hotwire probe was installed in the downstream of the cylinder at *X/D* = 5, *Y/D* = 3.5.

As seen from Fig. 13(a), the vortex shedding frequencies for all *U* values have similar variations with increasing α. The vortex shedding frequency for a given *U* increases with increasing α, reaching a maximum at α = 15°, followed by a drop for subsequent rise in α. The trend of the vortex shedding frequency variation in the present investigation is qualitatively similar to that by Huang *et al*. (2010) and Sohankar *et al*. (2015) for the infinite cylinder.

The previous research (Huang *et al*. 2010, Sohankar *et al*. 2015, Rockwell 1977, Obasaju 1983) reported for an infinite cylinder that the occurrence of maximum *St* is related to the reattachment of the separated shear layer. The shear layer deflects at the reattachment point near the downstream corner of the cylinder and then rolls up at a distance downstream of the body to form a narrow wake containing weaker vortices. The narrow wake suggests a contraction of the distance between the shed vortices in both transverse and longitudinal directions, leading to a higher shedding frequency.

Fig. 13(b) shows variations in vortex shedding frequency with freestream velocity for various α. For a

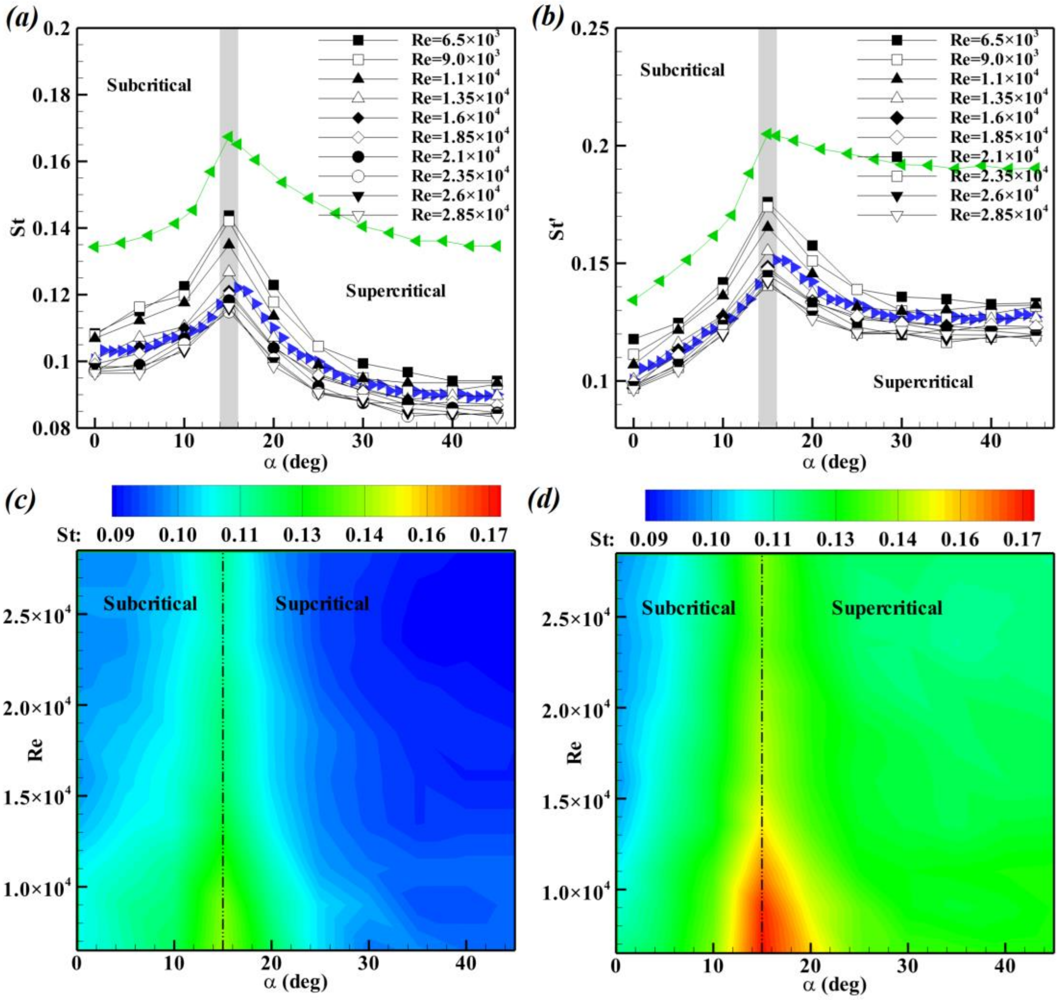

Fig. 14 Strouhal number based on (a, c) cylinder width D, and (b, d) projected width of the cylinder $D\sin\alpha+D\cos\alpha$. ▶, McClean and Sumner (2014, finite prism); ◀, Huang *et al*. (2010, infinite prism)

given α, the vortex shedding frequency increases almost linearly with increasing U, regardless of subcritical or supercritical region. The vortex shedding frequency data presented in Fig. 13 are converted to Strouhal numbers, i.e., St based on D and St' based on the projected width ($D\sin\alpha+D\cos\alpha$) of the cylinder on the cross-stream plane (Fig. 14). The use of projected width as the length scale for Strouhal number has been used for non-circular objects, for instance, a flat plate, airfoil, oval, wedge, etc. (Huang *et al*. 2010, Sohankar *et al*. 2015). In fact, the projection width has a link with the wake width of such bodies.

In Figs. 14(a) and 14(b), the results are plotted as functions of Re and α and compared with those of Huang *et al*. (2010) for an infinite square prism and McClean and Sumner (2014) for a finite square prism of AR = 7. Figs. 14(c) and 14(d) displays contours of St and St' values presented in Figs. 14(a) and 14(b), respectively.

Figs. 14(a) and 14(c) shows that, for the infinite square prism, the St is clearly sensitive to α. Based on the results reported in the literature, the maximum St for a finite prism occurs at α_{cr} = 15° - 17° that is dependent on experimental conditions (McClean and Sumner 2014). As shown in Fig. 14 (a), the St increases with increasing α from α = 0° to 15°, which is followed by a gradual fall up to α = 30°. The St approximately levels off for α > 30°. The finite prism data of McClean and Sumner (2014) for AR = 7 reveal that a maximum St or St' value occurs at α = 16°, which is in good agreement with the present results. Fig. 14(a) also demonstrate that the Strouhal number is higher for a finite prism than for an infinite prism at any α (Huang *et al*. 2010). Based on Fig. 14, the lowest value of Strouhal number occurs at α = 45° or at α = 0° when D (Fig. 14(a)) or $D\sin\alpha+D\cos\alpha$ (Fig. 14(b)) is used as the reference length scale, respectively. Fig. 14 also illustrates the Strouhal number slowly decreases as the Re increases. These differences become small for higher Reynolds numbers, where the St approximately approaches to same value for $Re > 15\times10^3$.

5. Conclusions

An experimental investigation was conducted on the flow field over a surface-mounted square prism of aspect ratio AR = 7. The experiments were carried out in a low-speed wind tunnel at Reynolds numbers Re = 6.5×10^3 -

28.5×10^3. The ratio of the boundary layer thickness to the prism height is $\delta/H = 0.07$. The effect of incidence angle α (= 0^o - 45^o) on the wake structure and Strouhal number is addressed.

As to the wake structure, a downwash flow from the free end of the prism is observed. The downwash flow extends to the mid-height of the prism, resulting in an increase in velocity near the wake centerline. The streamwise size of the wake region shrinks from the ground plane to the free end because of the mutual interaction between spanwise vortex, downwash flow and upwash flow. In addition, the wake width of the finite square prism changes with α, with minimum and maximum wake widths taking place at α =15^o and 45^o, respectively.

Similar to that for the infinite square prism, the turbulence intensity in the wake is sensitive to α. In contrast to the infinite prism for which the maximum turbulence intensity occurs in the shear layers from the lateral sides, the finite square prism generates the maximum turbulence intensity in the shear layers separated from the free edge and in the wake of the prism. While the former is attributed to the strong three-dimensional flow over the free end, the latter is ascribed to the downwash flow in the wake.

The results show that there is a dominant vortex-shedding frequency for all α values, and Strouhal number does not change along cylinder height. The critical α is found to be 15^o that separates the subcritical and supercritical regimes. The Strouhal number reaches a maximum when the wake width is minimum. The physical reason for this phenomenon is connected to separation bubble formation and the shear layer reattachment on the lateral side of the prism.

There are some similarities of the aerodynamic parameters between the finite and infinite prisms, mostly in their trends, not values. For example, the trends of variations in frequency, Strouhal number and wake width are similar for both prisms while their values are different. On the other hand, the critical α at which the Strouhal number and wake width reach a maximum and a minimum, respectively, is the same for both cylinders. In addition, the Strouhal number is smaller for the finite prism than for the infinite prism for all α values considered.

References

Alam, M.M., Zhou, Y. and Wang, X.W. (2011), "The wake of two side-by-side square cylinders", *J. Fluid Mech*., **669**, 432-471.

Alam, M.M., Bai, H.L. and Zhou, Y. (2016), "The wake of two staggered square cylinders", *J. Fluid Mech*., **801**, 475-507.

Adaramola, M.S., Akinlade, O.G., Sumner, D., Bergstrom, D.J. and Schenstead, A.J. (2006), "Turbulent wake of a finite circular cylinder of small aspect ratio", *J. Fluid. Struct*., **22**(6-7), 919–928.

Bourgeois, J.A., Sattari, P. and Martinuzzib, R.J. (2011), "Alternating half-loop shedding in the turbulent wake of a finite surface-mounted square cylinder with a thin boundary layer", *Phys. Fluids,* **23**, 095101, 1-15.

Brun, C., Aubrun S., Goossens, T. and Ravier, Ph. (2008), "Coherent structures and their frequency signature in the separated shear layer on the sides of a square cylinder", *J. Flow, Turbul. Combust*., **81**(1-2), 97-114.

Bruun, H.H. (1996), "Hot-wire anemometry, principles and signal analysis", OXFORD UNIVERSITY PRESS

Chen, J.M. and Liu, C.H. (1999), "Vortex shedding and surface pressures on a square cylinder at Incidence to a uniform Air Stream", *Int. J. Heat Fluid Fl*., **20**, 592–597.

Dutta, S., Muralidhar, K. and Panigrahi, P.P. (2003), "Influence of the orientation of a square cylinder on the wake properties", *Exp. Fluids*, **34**, 16-23.

Huang, R.F., Lin, B.H. and Yen, S.C. (2010), "Time-averaged topological flow patterns and their Influence on vortex shedding of a square cylinder in cross flow at Incidence", *J. Fluid. Struct*., **26**(3), 406-429.

Igarashi, T. (1984), "Characteristics of the flow around a square prism", *Bull. JSME*, **27**, 1858-1865.

Jorgenson, F. (2002), "How to measure turbulence with hot-wire anemometers" (A Practical Guide), Dantec Dynamics, Skovlunde, Denmark.

Lee, B.E. (1975), "The effect of turbulence on the surface pressure field of a square prism", *J. Fluid Mech*., **69**, 263-282.

Lim, H.C. Castro, I.P. and Hoxey, R.P. (2007), "Bluff bodies in deep turbulent boundary layers: Reynolds-number issues", *J. Fluid Mech*., 571, 97-118.

Lyn, D.A., Einav, S., Rodi, W. and Park, J.H. (1995), "A laser-doppler velocimetry study of ensemble-averaged characteristics of the turbulent near wake of a square cylinder", *J. Fluid Mech*., **304**, 285-319.

McClean, J.F. and Sumner. D. (2014), "An experimental investigation of aspect ratio and incidence angle effects for the flow around surface-mounted finite-height square prisms", *J. Fluid. Eng*., **136**, 081206, 1-10.

Minguez, M., Brun, C., Pasquetti, R. and Serre, E. (2011), "Experimental and high order LES analysis of the near wall flow over a square cylinder", *Int. J. Heat Fluid Fl*., **32**(3), 558-566.

Norberg, C. (1993), "Flow around rectangular cylinders: Pressure forces and wake frequencies", *J. Wind Eng. Ind. Aerod*., **49**(1-3), 187-196.

Obasaju, E.D. (1983), "An investigation of the effects of incidence on the flow around a square section cylinder", *J. Aero. Quart*., **34**(11), 243-259.

Okajima, A. (1982), "Strouhal numbers of rectangular cylinders", *J. Fluid Mech*., **123**, 379-398.

Okamoto, H., and Sunabashiri, Y. (1992), "Vortex shedding from a circular cylinder of finite length placed on a ground plane", *J. Fluids Eng*., **114**(4), 512-521.

Oudheusden, B.W.V., Scarano, F., Hinsberg, N.P.V. and Roosenboom, E.W.M. (2008), "Quantitative visualization of the flow around a square-section cylinder at incidence", *J. Wind Eng. Ind. Aerod*., **96**(6-7), 913-922.

Park, C.W. and Lee, S.J. (2000), "Free end effects on the near wake flow structure behind a finite circular cylinder", *J. Wind Eng. Ind. Aerod*., **88**(2-3), 231- 246.

Rastan, M.R., Sohankar, A. and Alam, M.M. (2017), "Low-Reynolds-number flow around a wall-mounted square cylinder: flow structures and onset of vortex shedding", *Phys. Fluids*, **29**, 103601, 1-19.

Rockwell, D.O. (1977), "Organized fluctuations due to flow past a square cross section cylinder", *J. Fluids Eng*., **99**(3), 511-516.

Sakamoto, H. and Arie, M. (1983), "Vortex shedding from a rectangular prism and a circular cylinder placed vertically in a turbulent boundary layer", *J. Fluid Mech*., **126**, 147-165.

Sakamoto, H. (1985), "Aerodynamic forces acting on a rectangular prism placed vertically in a turbulent boundary layer", *J. Wind Eng. Ind. Aerod*., **18**(2), 131-151.

Sarode, R.S., Gai, S.L. and Ramesh, C.K. (1981), "Flow around circular- and square-section models of finite height in a turbulent shear flow", *J. Wind Eng. Ind. Aerod*., **8**(3), 223-230.

Sohankar, A., Norberg, C. and Davidson, L. (1998), ‘‘Low-Reynolds number flow around a square cylinder at incidence: Study of blockage, onset of vortex shedding and outlet boundary condition”, *Int. J. Numer. Meth. Fl.*, **26**, 39-56.

Sohankar, A., Norberg, C. and Davidson, L. (1999), “Simulation of unsteady 3D flow around a square cylinder at moderate Reynolds number”, *Phys. Fluids*, **11**(2), 288-306.

Sohankar, A., Davidson, L. and Norbeg, C. (2000), “Large eddy simulation of flow past a square cylinder: comparison of different subgrid scale models”, *J. Fluid. Eng*., **122**(1), 39-47.

Sohankar, A. (2006), “Flow over a bluff body from moderate to high Reynolds numbers using large eddy simulation”, *Comput. Fluids*, **35**(10), 1154-1168.

Sohankar, A. (2008), “Large eddy simulation of flow past rectangular section cylinders: Side ratio effects”, *J. Wind Eng. Ind. Aerod*., **96**(5), 640-655.

Sohankar, A., Mohagheghian, S., Dehghan, A.A. and Dehghan Manshadi, M. (2015), “A smoke visualization study of the flow over a square cylinder at incidence and tandem square cylinders”, *J. Visualization*, **18**(4), 687-703.

Sumner, D., Heseltine, J.L. and Dansereau, O.J.P. (2004), “Wake structure of a finite circular cylinder of small aspect ratio”, *Exp. Fluids*, **37**(5), 720-730.

Trias, F.X. Gorobets, A. and Oliva A. (2015). “Turbulent flow around a square cylinder at Reynolds number 22,000: A DNS study”, *Comput. Fluids*, **123** (22), 87-98.

Wang, H.F., Zhou, Y., Chan, C.K., Wong, W.O. and Lam., K.S. (2004) “Flow structure around a finite length square prism”, *Proceedings of the 15th Australasian Fluid Mechanics Conference*, The University of Sydney, Sydney, Australia.

Wang, H.F., Zhou, Y., Chan, C.K. and Lam, K.S. (2006), “Effect of initial conditions on interaction between a boundary layer and a wall-mounted finite-length-cylinder wake”, *Phys. Fluids*, **18**, 065106, 1-12.

Wang, H.F. and Zhou, Y. (2009), “The finite-length square cylinder near wake”, *J. Fluid Mech*., **638**, 453-490.

West, G.S. and Apelt, C.J. (1982), “The effects of tunnel blockage and aspect ratio on the mean flow past a circular cylinder with Reynolds numbers between 10^4 and 10^5”, *J. Fluid Mech*., **114**, 361-377.

Williamson C.H.K. (1996), “Three-dimensional wake transition”, *J. Fluid Mech*., **328**, 345-407.

Yavuzkurt, S. (1984), “A guide to uncertainty analysis of hot-wire data”, *J. Fluid. Eng*., **106**(2), 181-186.

Yen, S.C. and Yang, C.W. (2011), “Flow patterns and vortex shedding behavior behind a square cylinder”, *J. Wind Eng. Ind. Aerod*., **99**(8), 868-878.

Yen, S.C. and Yang, C.W. (2012), “Characteristic flow field behind a square-cylinder using upstream mesh fences”, *J. Fluid. Eng*., **134**(9), 091202-1-9.

Zdravkovich, M.M. (2003), “Flow around circular cylinders”, **2**, Applications. Oxford University Press.

Zheng, Q.M. and Alam, M.M. (2017), “Intrinsic features of flow past three square prisms in side-by-side arrangement”, *J. Fluid Mech*., **826**, 996-1033.